Materials Science Research International, Vol.7, No.1 pp.19-26 (2001)

General paper

Simulation of the Forging Process Incorporating Strain-Induced Phase Transformation Using the Finite Volume Method (Part I; Basic Theory and Numerical Methodology)

Peiran DING*, Tatsuo INOUE**, Shoji IMATANI**, Dong-Ying JU*** and Edwin de VRIES ****
*Technical Division, MSC.Software Japan Ltd., 2-39, Akasaka 5-Chome, Minato-ku, Tokyo, Japan
**Department of Energy Conversion Science, Kyoto University, Sakyo-ku, Kyoto, Japan
***Department of Mechanical Engineering, Saitama Institute of Technology, Fusaiji 1690, Okabe, Saitama, Japan
****MSC.Software (E.D.C.) B.V., Groningenweg 6, 2803 PV, Gouda, The Netherlands

Abstract: A method to simulate the forging process and corresponding strain-induced austenitic-martensite phase transformation is formulated in the Eulerian description and its feasibility is examined. The method uses finite volume meshes for tracking material deformation and an automatically refined facet surface to accurately trace the free surface of the deforming material. By means of this finite volume method, an approach has been developed in the framework of *metallo-thermo-mechanics* to simulate metallic structure, temperature and stress/strain in the forging process associated with phase transformation. The incremental expression on the formulation of the kinetics equation is derived from Tsuta and Cortes' model. A mixture rule is adopted to evaluate the aggregate flow stress of the austenite-martensite affected by the respective flow stresses and phase transformation. This approach has been implemented in the commercial computer program MSC.SuperForge. This is the first report in which the fundamental framework is stated and the applicability of the developed method is confirmed using experimental results of the forging of a cylindrical billet. Some practical forging applications are demonstrated in the second report.

Key words: *Finite volume method, Explicit time integration, Strain-induced phase transformation, Incremental formulation of kinetics equation, Metallo-thermo-mechanics, Forging, SUS304 stainless steel*

1. INTRODUCTION

The properties of austenitic stainless steels, their high formability, strength and excellent corrosion resistance, are of great interest for architectural, automotive, and industrial applications. In some austenitic stainless steels such as SUS304, an austenitic-martensite phase transformation is induced by large deformation (plastic strain) during the forging process, according to the strain value and temperature. The strain-induced austenitic-martensite phase transformation can be developed at low temperature above M_s and almost completely inhibited at higher temperature M_d within usual strain ranges. The M_s signifies the temperature, at which the austenite starts to transform spontaneously to martensite in cooling, while M_d is the temperature above which deformation stresses/strains cannot initiate the transformation. Mechanical deformation can generate heat by the dissipation of plastic work. Due to this deformation and heat conduction, a temperature gradient develops in the workpiece. The variation of strain and temperature in the workpiece would affect the extent of martensite transformation.

An extensive investigation of strain-induced transformation behavior of SUS304 stainless steel by Angel [1] has shown that the transformation curve (volume fraction of martensite with respect to plastic strain at steady temperature) is sigmoidal in shape. He also proposed an empirical expression consistent with the sigmoidal shape. Since then, researches of kinetics of strain-induced transformation have been developed [2-10]. All of these theories and experiments suggest that the volume

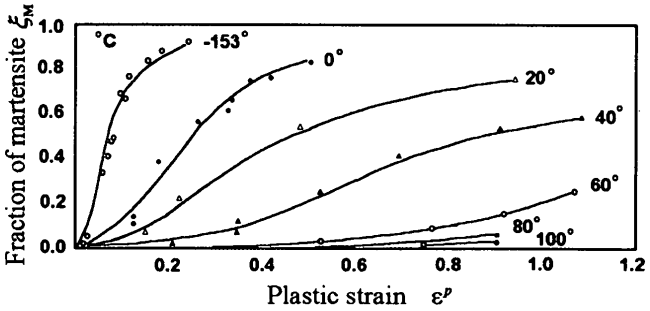

Fig. 1. Martensite content vs. plastic strain at various temperature [6].

fraction of martensite generated during deformation is a continuous function of strain (rather than stress) and temperature (Fig. 1 [6]). The parameters in these equations are found to give agreement between the experimental data and proposed model.

Olson and Cohen [2] established the kinetics of strain-induced transformation based on Angel's data by the shear-band intersection mechanism. Hecker et al. [3] examined the results in terms of Olson and Cohen's theory and proposed an extension of their theory to predict the transformation kinetics under multi-axial loading. According to them, it is appropriate to use Mises equivalent strain instead of the uni-axial strain used in Olson and Cohen's model. Tomita et al. [4] continued to enhance this model by taking strain rate dependency into account.

Received September 12, 2000
Accepted February 6, 2001

Ludwigson and Berger [5] studied the main factors, which affect such transformation and plastic behavior. A transformation model was formulated accounting for the observed autocatalytic nature of martensite formation, that is, the ability of martensite to accelerate the formation of additional martensite. Tsuta and Cortes [6,7] have modified Ludwigson's model by using the characteristic strain concept, which can be expressed as a function of temperature.

Kawai et al. [8] expressed the kinetics of strain-induced transformation in incremental form with respect to strain and temperature. Shinagawa, Nishikawa, Ishikawa and Y. Hosoi [9] formulated the kinetics of strain-induced transformation in the incremental form as a function of temperature. Autocatalytic nature of martensite formation is taken into account in both of the models.

During the forging process, the aggregate flow stress of the austenite-martensite is affected by the respective flow stresses and phase transformation. As a result of martensite phase transformation, the hardening can increase rapidly with the deformation of the material during the forging process. So that the flow stress in these unstable stainless steels strongly depends on the martensite content in the material. The relationship between the flow stress and martensite phase transformation in austenitic stainless steels becomes very important.

The stainless steel industry has to control the mechanical properties to final products and to estimate the forging process in advance of operation. Improved formability in austenitic stainless steels might be achieved through an improved understanding of their behavior on phase transformation and flow stress. Such information may be obtained by numerical simulation.

Thus far, a number of noticeable and successful simulations of the structural changes of the material during the forging processes [4,7,9] by employing the implicit finite element method based on Lagrangian formulation have been reported. However, those simulations are in most cases related to the forging processes of relatively simple shapes using two-dimensional models. One of the most notable barriers is the remeshing technology, which is the bottleneck for finite element methods in complicated three-dimensional forging. For the manufacturing process such as forging where metal is under large plastic deformation, the finite element method sometimes exhibits weaknesses, which must be carefully monitored:

- Finite element meshes usually get over-distorted; auto-remeshing is then necessary to complete the simulation. But the auto-remeshing technology for three-dimensional problems is not so robust and also very time consuming.
- Even for two-dimensional elastic-plastic problems, the remeshing may lead to erroneous results [11]. Each remeshing step will involve quite a lot of loss in volume, which is not acceptable for forging simulations.

When *strain-induced phase transformation* during the process of metal forming (large deformation like forging) is taken into account, the finite element method will encounter more difficulties in numerical stability beside remeshing and loss of volume.

The finite volume method [12,13] to simulate forging is adopted in this paper. The advantages of the finite element and the finite volume approaches are combined: it employs a fixed finite volume mesh for tracking material deformation and an automatically refined facet surface (material surface) to accurately trace the free surface of the deforming material. This is particularly suited for large three-dimensional material deformation such as forging since remeshing techniques are not required. A new solution strategy of the time integration is presented in order to stabilize the numerical calculation.

By means of this finite volume method, a new approach based on the *metallo-thermo-mechanics* [14,15] to simulate metallic structure, temperature and stress/strain in the three-dimensional forging process associated with strain-induced phase transformation has been introduced. The material is considered as elastic-plastic and takes into account the phase transformation effects on the yield stress. The temperature increase due to plastic deformation, heat conduction in the workpiece and dies, heat transfer between workpiece/die and ambient and thermal stress has been analyzed simultaneously. Strain-induced phase transformation, latent heat, transformation stress and strain are included. At present, the numerical simulation of forging associated with strain-induced phase transformation using the finite volume method is still pioneering work. Searching for publications on this subject in the open scientific literature gives no result. This approach has been implemented in the commercial computer program MSC.SuperForge. The applicability of the developed method is confirmed with experimental results.

2. BASIC THEORY

2.1. Mixture Law

In the following, the material parameters χ, such as thermal conductivity, specific heat, elastic modulus, yield stress, hardening modulus and so on, are assumed to be evaluated by the mixture law:

$$\chi = \sum \chi_I \xi_I , \tag{1}$$

where χ_I and ξ_I are the properties and the volume fraction of the I-th constituents, respectively. Hereunder, the summation Σ is taken for all constituents.

The kinetics equations for the fractions are developed under the restriction:

$$\sum \xi_I = 1 . \tag{2}$$

For SUS304 stainless steel, we consider only two volume fractions: austenite ξ_A and martensite ξ_M.

2.2. Kinetics of Strain-Induced Martensite Transformation

In this paper, Tsuta and Cortes' model is adopted as the basis of the kinetics model of martensite phase transformation for SUS304. This model describes the volume

of strain-induced transformation as a function of equivalent plastic strain $\bar{\varepsilon}^p$ and temperature T:

$$\xi_M = \left\{1+\left[\frac{\bar{\varepsilon}^p}{Ce^{-D/T}}\right]^{-B}\right\}^{-1}, \quad (3)$$

where material parameters B, C and D are determined by experiments as 2.11, 2847.0 and 2548.0, respectively.

2.3. Incremental Formulation of the Transformation Kinetics

Since material deforms under strong non-linear conditions, it is necessary to take into account the incremental expression on the formulation of the kinetics equation.

An incremental form can be derived from Eq.(3):

$$\dot{\xi}_M = \frac{\partial \xi_M}{\partial \bar{\varepsilon}^p}\dot{\bar{\varepsilon}}^p + \frac{\partial \xi_M}{\partial T}\dot{T}, \quad (4)$$

where

$$\frac{\partial \xi_M}{\partial \bar{\varepsilon}^p} = B\left\{Ce^{-D/T}\left[1+\left(\frac{\bar{\varepsilon}^p}{Ce^{-D/T}}\right)^{-B}\right]^2\left(\frac{\bar{\varepsilon}^p}{Ce^{-D/T}}\right)^{B+1}\right\}^{-1}, \quad (5)$$

$$\frac{\partial \xi_M}{\partial T} = -BD\bar{\varepsilon}^p\left\{CT^2e^{-D/T}\left[1+\left(\frac{\bar{\varepsilon}^p}{Ce^{-D/T}}\right)^{-B}\right]^2\left(\frac{\bar{\varepsilon}^p}{Ce^{-D/T}}\right)^{B+1}\right\}^{-1}. \quad (6)$$

Since forging of this type of stainless steel is usually performed at room temperature, martensite will never be transformed back to austenite under this condition. So that when $\dot{T} \geq 0$, then $\partial\xi_M/\partial T=0$. When $\dot{T}$ is negative (because of die chilling or heat transfer between material and environment), martensite can be generated from austenite; the effect of term $\partial\xi_M/\partial T$ should be taken into account as Eq.(6).

2.4. Heat Conduction Equation

Strain-induced transformation is strongly dependent on the temperature. The temperature field is affected by the heat generation converted from mechanical work and also the latent heat due to phase change. So the heat conduction equation is derived by considering the total energy balance while neglecting the small effect of heat generation due to elastic mechanical work [14]:

$$\rho c_p\dot{T} - \frac{\partial}{\partial x_i}\left(k\frac{\partial T}{\partial x_i}\right) - \sigma_{ij}\dot{\varepsilon}^p_{ij} + \sum \rho_l l_l \dot{\xi}_l = 0, \quad (7)$$

where c_p and k denote the specific heat and the coefficient of heat conduction. ρ_l is the density of the l-th constituent. l_l is the latent heat produced by the progressive l-th constituent with volume fraction ξ_l. σ_{ij} is Cauchy stress tensor.

In addition to the heat conduction within the material, heat transfer from the surface with unit normal n_i as a boundary condition is treated as:

$$k\frac{\partial T}{\partial x_i}n_i = -h(T)(T-T_c), \quad (8)$$

where $h(T)$ is the heat transfer coefficient, and T_c is the ambient or die temperature. The adiabatic boundary as h=0 is imposed on the symmetric axis.

2.5. Elastic Plastic Constitutive Equation

Within the infinitesimal theory of kinematics, the total strain rate can be divided into elastic, plastic, and thermal strain rates and those by structural dilatation due to phase transformation and transformation plasticity:

$$\dot{\varepsilon}_{ij} = \dot{\varepsilon}^e_{ij} + \dot{\varepsilon}^p_{ij} + \dot{\varepsilon}^T_{ij} + \dot{\varepsilon}^m_{ij} + \dot{\varepsilon}^{tp}_{ij}. \quad (9)$$

The elastic strain is given by Hooke's law:

$$\varepsilon^e_{ij} = \frac{1+\nu}{E}\sigma_{ij} - \frac{\nu}{E}\sigma_{kk}\delta_{ij}, \quad (10)$$

where E is Young's modulus and ν is Poisson's ratio. The thermal strain rate is:

$$\dot{\varepsilon}^T_{ij} = \alpha\dot{T}\delta_{ij}, \quad (11)$$

with the thermal expansion coefficient α. And the phase transformation strain rate is:

$$\dot{\varepsilon}^m_{ij} = \sum(\alpha_l(T-T_0)+\beta_l)\dot{\xi}_l\delta_{ij}, \quad (12)$$

where α_l is the thermal expansion coefficient of the l-th constituent and β is the dilatation due to structural change. T_0 means the reference temperature.

When introducing temperature and structural dependent yield function with hardening parameter κ:

$$F = F(\sigma_{ij}, \varepsilon^p_{ij}, \kappa, T, \xi_l), \quad (13)$$

then the plastic strain rate leads to:

$$\dot{\varepsilon}^p_{ij} = \Lambda\frac{\partial F}{\partial \sigma_{ij}}. \quad (14)$$

The isotropic hardening rule of Mises type is used here as the yield function F.

The strain rates due to transformation plasticity depend on the l-th constituent ξ_l in the form [16]:

$$\dot{\varepsilon}^{tp}_{ij} = \frac{3}{2}\sum K_l h(\xi_l)\dot{\xi}_l s_{ij}, \quad (15)$$

where

$$h(\xi_I) = 2(1-\xi_I), \tag{16}$$

and where s_{ij} is the deviatoric stress, and K_I is the intensity of transformation plasticity.

3. NUMERICAL METHODOLOGY

3.1. Outline of Finite Volume Method

In the case of Eulerian description, the governing equation, expressing the conservation of any physical quantity is formulated in the form:

$$\frac{\partial \boldsymbol{Q}}{\partial t} + \nabla \cdot \boldsymbol{F} = 0, \tag{17}$$

where $\boldsymbol{Q}$ is the variable and $\boldsymbol{F}=\boldsymbol{F}_{\text{convection}}+\boldsymbol{F}_{\text{diffusion}}$ is the corresponding flux, consisting of convection and diffusion terms.

Equation (17) gives the conservation laws of mass, momentum and energy, in which the variables and the corresponding fluxes are listed in Table 1. Here v_i is the velocity vector; h_i is the heat flux; e_t is the total energy per unit of mass given by $e_t=e+1/2v_jv_j$, with the internal energy per unit mass e. The body force is neglected throughout the present investigation.

By using the Gauss' divergence theorem, Eq.(17) is written in an integral form for a control volume V with a closed surface S, which is stationary within a total domain:

$$\frac{\partial}{\partial t}\int_V \boldsymbol{Q}\, dV + \int_S \boldsymbol{F}\cdot \boldsymbol{n}\, dS = 0. \tag{18}$$

Subdividing control volume V into disjunct finite volume elements, as illustrated in Fig. 2, $V^{I\pm1,J,K}$, $V^{I,J\pm1,K}$ and $V^{I,J,K\pm1}$ are neighboring elements of $V^{I,J,K}$. For simple implementation, the finite volume mesh is aligned with coordinate system axes. A straightforward and simple discretization in Cartensian coordinates is obtained by numerically integrating Eq.(18):

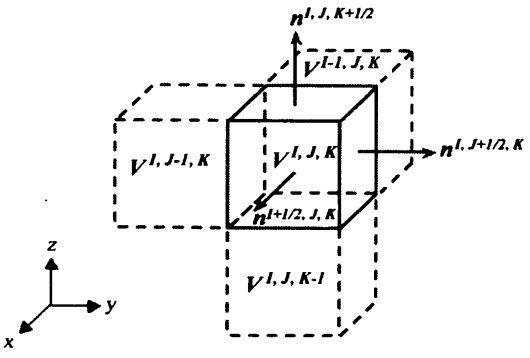

Fig. 2. Definition of finite volume.

Table 1. Variables and fluxes.

Conservation law		Mass	Momentum	Energy
$\boldsymbol{Q}$	variable	ρ	ρv_i	ρe_t
$\boldsymbol{F}$	convection	ρv_i	$\rho v_i v_j$	$\rho e_t v_i$
	diffusion	0	$-\sigma_{ij}$	$h_i - \sigma_{ij}v_j$

$$\begin{aligned}\Delta V^{I,J,K}\frac{\Delta Q^{I,J,K}}{\Delta t} = -(&F^{I+\frac{1}{2},J,K}\Delta S^{I+\frac{1}{2},J,K} - F^{I-\frac{1}{2},J,K}\Delta S^{I-\frac{1}{2},J,K} \\ &+ F^{I,J+\frac{1}{2},K}\Delta S^{I,J+\frac{1}{2},K} - F^{I,J-\frac{1}{2},K}\Delta S^{I,J-\frac{1}{2},K} \\ &+ F^{I,J,K+\frac{1}{2}}\Delta S^{I,J,K+\frac{1}{2}} - F^{I,J,K-\frac{1}{2}}\Delta S^{I,J,K-\frac{1}{2}}),\end{aligned} \tag{19}$$

where $\Delta V^{I,J,K}$ is the volume of the element $V^{I,J,K}$, $Q^{I,J,K}$ is the mean value of Q over $V^{I,J,K}$ and is collocated at the center of the finite volume element. The left part of the equation is the summation of the total fluxes normal to the surface $\Delta S^{I\pm1/2,J,K}$, $\Delta S^{I,J\pm1/2,K}$ and $\Delta S^{I,J,K\pm1/2}$ of the faces of $V^{I,J,K}$.

3.2. Solution Strategy

When the governing equations are integrated in time under the Eulerian description by an explicit dynamic procedure, we solve the complete system by separating the diffusion flux and convection flux respectively into an acoustic step and an advection step. The advantages of doing this are: 1) to avoid the non-linearity due to convection term when the impulse is evaluated, 2) to stabilize the numerical calculation, 3) to simplify the implementation. The iteration scheme is not employed for the interaction between the acoustic step and the advection step. The neglect should be minor with respect to the small time step in the explicit method.

In the acoustic step, the stress and impulse waves are assumed to propagate through the control volumes in the whole domain. The variation per unit time of the quantity in each volume is contributed from the diffusion flux through its surrounding faces.

In the advection step, by employing the new velocity updated in the acoustic step, the mass flows from one control volume to another and transports the corresponding properties (stress/strain, energy and material characteristics, etc.) without updating the physical quantity associated with the mass. This step exists only in the framework of the Eulerian formulation. In the Lagrangian formulation, the mass within an element remains constant, and therefore, as the mass moves, the element moves with the mass and so does the properties of the mass involved. In the Eulerian formulation the mass flows through a fixed computational domain. As a result, the properties of mass contained within an element change due to the mass flow from element to element.

3.2.1. Acoustic step

In this step only evolution of stress and impulse waves is provided, the contribution from the convection flux to the variation of the quantity in each volume will be taken care of in the advection step. Under the assumption that the mass density is constant in each control volume during one acoustic step, the conservation law of mass is satisfied automatically. The volume integral form for the impulse is found from the conservation law of momentum as:

$$\int_V \frac{\partial v_i}{\partial t} dV = \frac{1}{\rho} \int_S \sigma_{ij} n_j dS \,, \tag{20}$$

where n_i is the unit normal vector on the boundary S of the control volume V.

The values on faces of the control volume can be obtained by solving the Riemann problem [17]. Then the new velocity in the control volume is updated by using the velocity increment evaluated from Eq.(20).

The volume integral form for the conservation law of energy becomes:

$$\rho \int_V \frac{\partial e}{\partial t} dV - \int_V \sigma_{ij} \dot{\varepsilon}_{ij} dV = -\int_S h_i n_i dS \,. \tag{21}$$

The energy conservation law is used to derive the heat conduction equation, which has been described in section 2.4.

3.2.2. Advection step

In the advection step, the contribution from the convection flux to the variation of the quantity in each volume is evaluated. The material and corresponding properties are transported according to the velocity updated in the acoustic step without changing the value of the physical quantity associated with the material. The divergence of diffusion flux term in Eq.(17) disappears and mass, momentum and energy are transported as:

$$\frac{\partial(\rho\Phi)}{\partial t} + \frac{\partial(\rho\Phi v_i)}{\partial x_i} = 0 \,. \tag{22}$$

Other properties (stress/strain, material characteristics, e.g.) are transported in the same conservation form as Eq.(22). Here, Φ is any physical quantity per unit mass. The integral form to be used in the numerical advection scheme for the finite volume method reads:

$$\frac{D}{Dt} \int_V \rho\Phi dV = -\int_S \rho\Phi v_i n_i dS \,, \tag{23}$$

where material time derivative D/Dt is used for material particles transformation. Under the Eulerian description, since we fix the control volumes in a domain, the velocity of the volume (not v_i of the material particle) is zero. In this case D/Dt can be replaced by $\partial/\partial t$, so Eq.(18) also holds true in the advection step.

3.2.3. Update variables

The density is updated after the mass is transported. The strain rate tensor is calculated from the velocity increment evaluated in the acoustic step:

$$\dot{\varepsilon}_{ij} = \frac{1}{2}\left(\frac{\partial v_i}{\partial x_j} + \frac{\partial v_j}{\partial x_i}\right) . \tag{24}$$

With the strain rate tensor, the strain and stress status are determined from the elastic-plastic constitutive relations described in section 2.5. The temperature is determined by solving the heat conduction equation.

The phase transformation is then calculated according to the new temperature and strain fields.

All the variables in the governing equations are evaluated in a Runge-Kutta time integration scheme [17].

3.3. Automatic Surface Tracking

The shape of the deforming material is encapsulated by a geometric surface comprised of triangular facets. These facets are geometric entities rather than finite elements. The facet surface is constrained to move with the material in order to track the exact material surface and also precisely apply the boundary condition to the material. An algorithm called Resolution Enhancement Technology (RET) is employed to automatically refine the facet surface throughout the simulation to capture the continuously changing and the increasing complexity of the deforming material. Another task of RET is to refine the material facet surface at locations of the die(s) which have significant curvature. The facet surface must be capable of *folding* around the features of the die surface. Principally speaking, RET is a kind of two-dimensional remeshing technology from the geometry point of view [12]. Since the facets are geometric entities rather than finite elements, the common problems which are associated with finite elements based on remeshing algorithms, such as severe distortion and significant increase of computation time with a loss of accuracy, are avoided.

4. SIMPLE NUMERICAL SIMULATION

In order to verify the approaches described in the preceding chapters, we consider a simulation of the forging of a cylindrical billet. The experimental results by Shinagawa, Nishikawa, Ishikawa and Y. Hosoi [9] on the cylindrical billet forging are used. The material used in the experiments was SUS304 austenitic stainless steel. The martensite start temperature M_s is –216 °C [8] evaluated from the chemical compositions. The martensite inhibited temperature M_d should be higher than 100 °C according to [6]. A specimen is machined into a cylindrical billet of 11.2 mm diameter and 16.8 mm height and is pushed between two flat dies. In order to verify the three-dimensional ability of the program, the numerical model is generated in three dimensions shown in Fig. 3. Because of the axi-symmetric condition, a triangular prismatic mesh is used with head angle of 30 deg. Sym-

metry is assumed in the middle horizontal plane and only the upper quarter of the billet is modeled. The upper die is modeled as a rigid body and has the initial velocity as 0.025 mm/s and drops to zero linearly until the end of forging process. The stroke of the die is 4.0 mm. The initial temperatures of the billet and dies are 15 °C. A steady temperature of the environment is used as 15 °C.

Many investigations have shown that for SUS304 stainless steel the strain hardening in austenite state exhibits flow curves that can be described as:

$$\overline{\sigma}_A = K(\overline{\varepsilon}^p)^n . \tag{25}$$

The flow constant K depends on the equivalent strain rate [4]. On the other hand, the flow stress contribution of martensite may be defined as follows according to Ludwigson and Berger [5]:

$$\overline{\sigma}_M = C(\xi_M)^Q , \tag{26}$$

where n, C, Q are constants determined by experiment.

The latent heat generated in the course of austenite-martensite phase transformation, the volumetric dilatation due to structural change, and the intensity of austenite-martensite phase transformation plasticity are taken from [4], [14], and [16], respectively.

The heat transfer plays a very important role here because adiabatic heating can inhibit the transformation and thereby give influence on the plastic flow. The heat transfer coefficient between workpiece and die and between workpiece/die and ambient are taken from Tsuta and Cortes [10].

Coefficient of heat conduction, specific heat and elastic modulus, which are dependent upon the content of each phase and temperature, are shown in Fig. 4. The thermal expansion coefficient is taken as $1.5\text{x}10^{-5}$ 1/K for austenite and $1.1\text{x}10^{-5}$ 1/K for martensite. Here, the data of austenite is taken from [18] and [19]. Since the data of martensite for SUS304 is not available in the literature, data for carbon steel [14] is used with an assumption that the difference is minor.

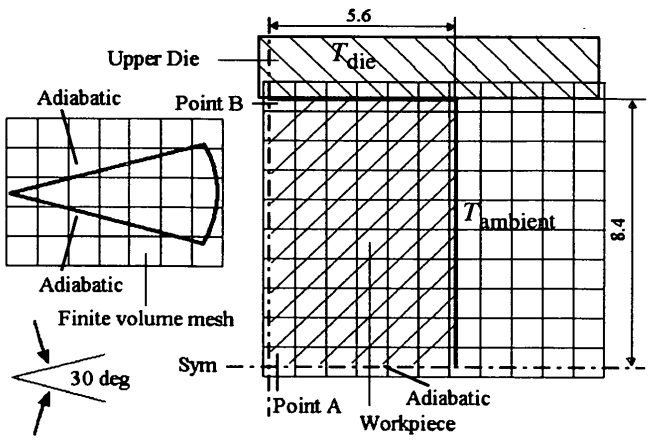

Fig. 3. Schematic illustration of numerical model.

5. ILLUSTRATION OF RESULTS AND DISCUSSION

Figure 5 shows the deformation modes of the billet for some representative strokes. The variation of the shape is successfully encapsulated by a geometric surface comprised of triangular facets.

The simulated results for temperature, equivalent plastic strain, the volume fraction of martensite, and equivalent stress are depicted in Figs. 6 (a), (b), (c) and (d) at points A and B during the forging stage. As shown in Fig. 3, point A is in the center of billet and point B is on the top surface of the billet in the axi-symmetric line.

The temperature at point A rises with the deformation because of the dissipation of plastic work. At point B, even though the plastic deformation is minor, the temperature rises 27 °C because of the heat conducted from the central part. The phase is transformed from austenite to martensite during the deformation. The more strain is gained, the more martensite increases with induced strain.

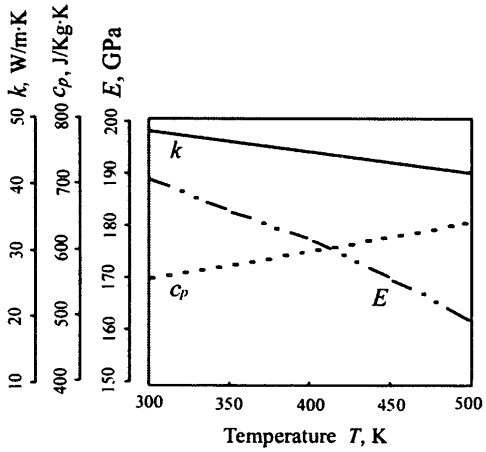

(a) Martensite

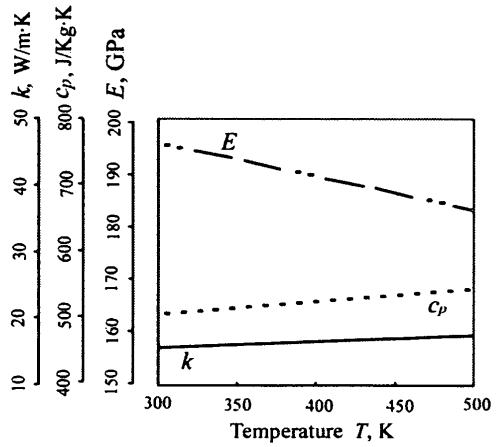

(b) Austenite

Fig. 4. Mechanical and thermo-physical material properties of SUS304.

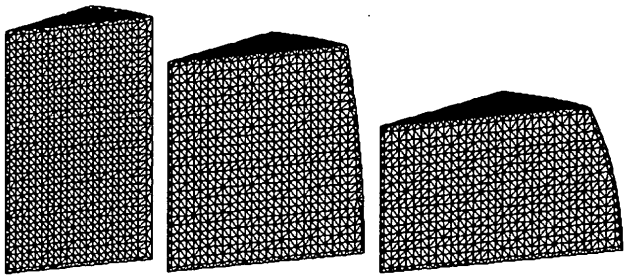

0 mm (initial) 2 mm (middle) 4 mm (final)

Fig. 5. Deformation modes of the billet with progressive stroke.

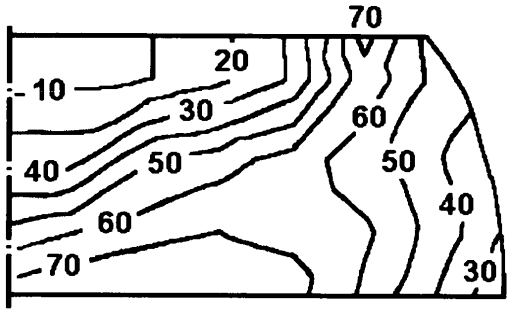

(a) Measured [9]

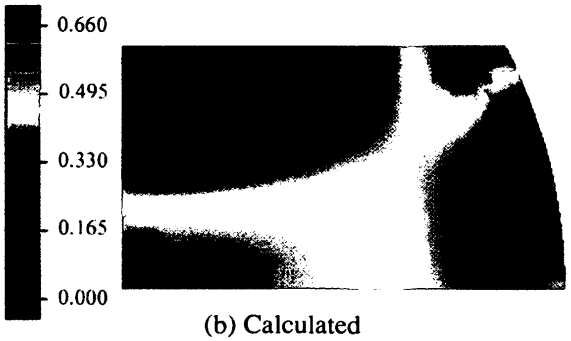

(b) Calculated

Fig. 7. Experimental measured and calculated martensite distribution at the end of the process.

Fig. 8. Calculated equivalent stress distribution at the end of the process.

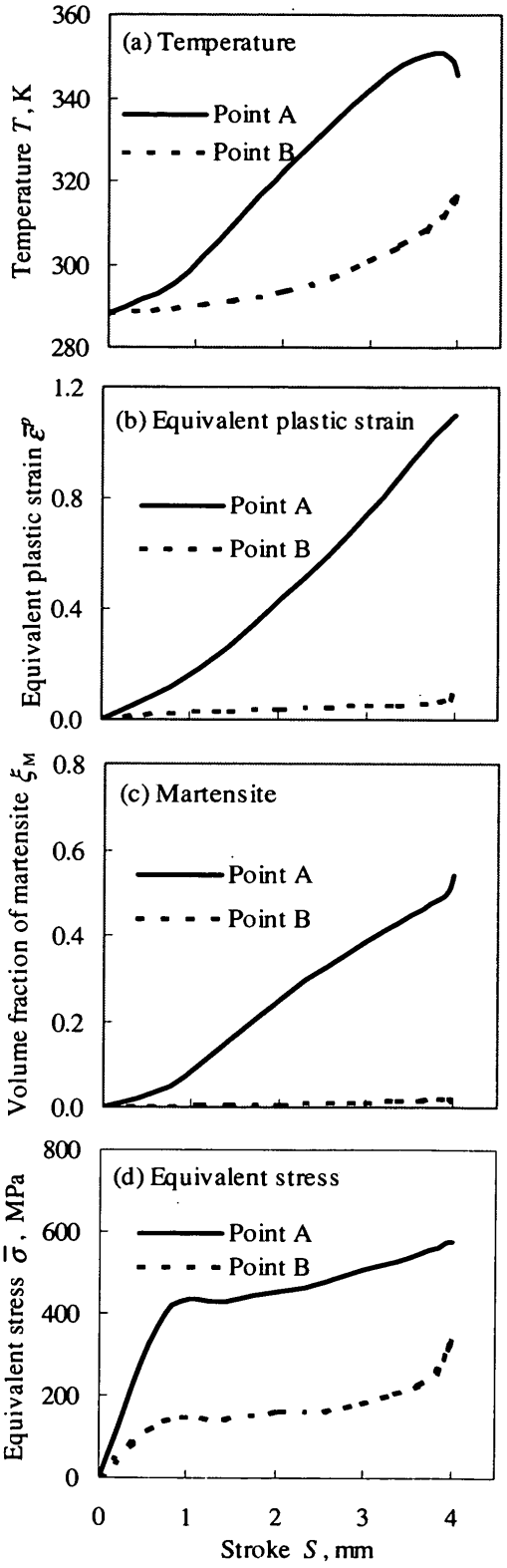

Fig. 6. Variation of temperature, equivalent plastic strain, volume fraction of martensite, equivalent stress with progressive stroke at Point A and B.

The experimental measured and calculated martensite distributions at the end of the process are compared in Fig.7. The martensite distribution in the experiment is obtained by a coupled usage of magnetic measurement and X-ray diffraction [9]. The simulation successfully grasps the martensite transformation and shows a good agreement in tendency with the experimental ones.

The simulated equivalent stress distribution at the end of the process is plotted in Fig. 8. We find that the region with high stress concentration coincides with the high volume fraction of martensite phase transformation.

6. CONCLUSION

The finite volume method using Eulerian formulation is applied to simulate forging coupled with strain-induced phase transformation. The deforming workpiece flows through fixed finite volume meshes. This is particularly suited for large three-dimensional material deformation such as forging since remeshing techniques are not required. The incremental expression on the formulation of the kinetics equation is derived from Tsuta and Cortes' model. The coupled *metallo-thermo-mechanics* system to simulate metallic structure, temperature and stress/strain has been extended to large deformation. A mixture rule is adopted to evaluate the aggregate flow stress of the austenite-martensite affected by the respective flow stresses and phase transformation. To demonstrate the feasibility of this method a three-dimensional simulation of a cylindrical billet forging has been used as an example. The simulation results show a good agreement in tendency with the experimental ones.

Attention has to be paid to the influence of strain rate on austenitic-martensite phase transformation and the consequently the aggregate stress. The results of this study constitute Part II.

Acknowledgments – The authors gratefully express their appreciation to Professor T. Tsuta, Hiroshima University, Professor T. Ishikawa, Nagoya University, for their kind provision of experimental data.

REFERENCES

1. T. Angel, J. Iron Steel Inst., **177** (1954) 165.
2. G.B. Olson and M. Cohen, Met. Trans. A, **6A** (1975), 791.
3. S.S. Hecker, M.G. Stout, K.P. Staudhammer and J.L. Smith, Met. Trans. A, **13A** (1982) 619.
4. Y. Tomita and T. Iwamoto, Int. J. Mech. Sci., **37** (1995) 1292.
5. D.C. Ludwigson and J.An. Berger, J. Iron Steel Inst., **207** (1969) 63.
6. J. A. Cortes R., T. Tsuta, Y. Mitani and K. Osakada, JSME Int. I, **35** (1992) 201.
7. T. Tsuta and J. A. Cortes R., JSME Int. A, **36** (1993) 63.
8. N. Kawai, H. Saiki and H. Hirate, J. of the Japan Soc. Tech. Plasticity, **17** (1976) 899 (in Japanese).
9. K. Shinagawa, H. Nishikawa, T. Ishikawa and Y. Hosoi, Iron and Steel, **3** (1990) 156 (in Japanese).
10. J. A. Cortes R. and T. Tsuta, Memoirs of the Faculty of Engineering, Hiroshima University, **11**-3 (1993) 35.
11. A. E. Tekkaya, Proc. 30th Plenary Meeting of the International Cold Forging Croup ICFG, (1997) 1.
12. W.J. Slagter, C.J.L Florie and A.C.J. Venis, Proc. of the 15th National Conference on Manufacturing Research, (1999) 73.
13. P. Ding, D.Y. Ju, T. Inoue and E. de Vries, Acta Metall. Sinica. (Eng. Lett.), **1** (2000) 270.
14. T. Inoue, S. Nagaki, T. Kishino and M. Monkawa, Ing. Arch., **50** (1981) 315.
15. T. Inoue, Thermal Stresses III, Elseiver Science Publishers B.V. (1989) 192-278.
16. M. Miyao, Z.G. Wang and T. Inoue, J. Soc. Mat. Sci., **35** (1986) 1352 (in Japanese).
17. C. Hirth, Numerical Computation of Internal and External Flows, Volume 2: Computational Methods for Inviscid and Viscous Flows, John Wiley & Sons (1990).
18. D.Y. Ju, T. Inoue and H. Matsui, Advances in Engineering Plasticity and its Applications, Elsevier Science Publishers (1993) 521.
19. I. Ohnaka, Introduction of Heat Transfer and Solidification Analysis – Application on Casting Process, Maruzen Publisher (1985) (in Japanese).